Int. J. Heat Mass Transfer. Vol. 29, No. 6, pp. 889–898, 1986
Printed in Great Britain

0017–9310/86 $3.00 + 0.00
Pergamon Journals Ltd.

Numerical analysis of natural convection in a rectangular enclosure horizontally divided into fluid and porous regions

TATSUO NISHIMURA,* TORU TAKUMI,* MITSUHIRO SHIRAISHI,* YUJI KAWAMURA* and HIROYUKI OZOE†

* Department of Chemical Engineering, Hiroshima University, Higashi-Hiroshima 724, Japan
† Department of Industrial and Mechanical Engineering, Okayama University, Okayama 700, Japan

(*Received* 19 *December* 1985)

Abstract—This paper describes an analytical study of laminar natural convection heat transfer in a rectangular enclosure horizontally divided into fluid and porous regions. The Navier–Stokes equation governs the fluid motion in the fluid region, while Brinkman's extension of Darcy's law is assumed to hold within the porous region. These equations are solved using a finite-element method in the range $10^3 \leqslant Ra_f \leqslant 10^5$ and $10^{-3} \leqslant Da \leqslant 10^{-5}$. The experiment is also performed using a rectangular enclosure filled with silicone oil and glass beads. It is shown that the flow pattern, temperature distribution and Nusselt number obtained from the numerical calculation satisfactorily predict the experimental data.

1. INTRODUCTION

NATURAL convection induced by buoyancy effects in an enclosed space filled either with a fluid or a fluid-saturated, porous medium has attracted considerable attention over the past decade [1–5]. Interest in this fundamental topic has been fuelled by applications to many real-life situations ranging from thermal insulation engineering to geothermal engineering. Recently various studies on natural convection in either multiple fluid layers or porous layers have been developed to determine the effect of inhomogeneity on the heat transfer [6–10]. However, the investigation of natural convection in a system consisting of both a fluid layer and a fluid-saturated, porous layer is quite limited.

Somerton and Catton [11] presented the analytical prediction of the onset of convection for a system consisting of a volumetrically heated, porous medium saturated with and overlaid with a fluid, heated or cooled from below. Tong and Subramanian [12] analyzed natural convection in rectangular enclosures that are vertically divided into a region filled with a fluid and a region filled with a fluid-saturated, porous medium. Two regions are separated by an impermeable wall without the thermal resistance and both side walls of the enclosure are heated and cooled, respectively. They reported that even the enclosure partially filled with a porous medium has a heat transfer rate identical to that of a fully porous enclosure when the porous portion of the enclosure is more than about 0.5. Nishimura *et al.* [13] experimentally investigated natural convection in rectangular enclosures heated and cooled from a side, respectively. The upper part of the enclosure is filled with water and the lower part is filled with a water-saturated, porous medium of glass beads as shown in Fig. 1. Nishimura *et al.* presented the heat transfer correlation with a function of the porous portion of the enclosure and also discussed the natural convection mechanism by the flow visualization and the temperature distribution in the enclosure.

In this paper, we analyze natural convection for the same system as that of our previous experimental study [13]. The two-dimensional, Navier–Stokes equation governs the fluid motion in the fluid region, while Brinkman's extension of Darcy's law [14] is assumed to hold within the porous region. These equations have been solved using a finite-element method, and the effects of Rayleigh number and Darcy number on the

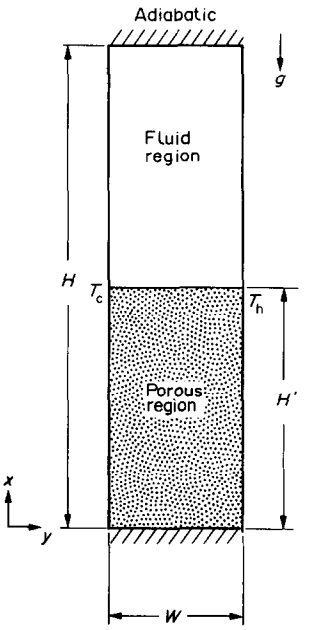

FIG. 1. Schematic diagram of enclosure partially filled with a porous medium.

NOMENCLATURE

C_{pf} specific heat of the fluid
Da Darcy number, κ/W^2
g gravitational acceleration
H height of the enclosure
H' height of the porous region
h heat transfer coefficient
Nu_e Nusselt number, hW/λ_e
Nu_f Nusselt number, hW/λ_f
$\overline{Nu}_f$ Nusselt number when natural convection occurs independently in the fluid and porous regions
Nu_f^* Nusselt number based on fluid thermal conductivity for a fully fluid enclosure with an aspect ratio of $(H-H')/W$
Nu_p^* Nusselt number based on effective thermal conductivity for a completely porous enclosure with an aspect ratio of H'/W
P dimensionless pressure, $pW^2/(\rho_f\alpha_f^2)$
p pressure
Pr_f Prandtl number of the fluid
Ra_e Rayleigh number, $g\beta(T_h-T_c)W^3/(\alpha_e\nu_f)$
Ra_e^* Rayleigh number, Ra_eDa
Ra_f Rayleigh number, $g\beta(T_h-T_c)W^3/(\alpha_f\nu_f)$
S size of secondary circulation because of the numerical error
T temperature
T_c temperature at the cold wall
T_h temperature at the hot wall
U dimensionless vertical velocity, uW/α_f
u vertical velocity
V dimensionless horizontal velocity, vW/α_f
v horizontal velocity
W width of the enclosure
X dimensionless vertical coordinate, x/W
x vertical coordinate
Y dimensionless horizontal coordinate, y/W.

Greek symbols
α_e thermal diffusivity of the porous medium, $\lambda_e/(\rho_fC_{pf})$
α_f thermal diffusivity of the fluid, $\lambda_f/(\rho_fC_{pf})$
β volumetric expansion coefficient
ζ shear stress
θ dimensionless temperature, $(T-T_c)/(T_h-T_c)$
κ permeability
λ_e effective thermal conductivity of the porous medium
λ_f thermal conductivity of the fluid
μ_f viscosity of the fluid
ν_f kinematic viscosity of the fluid
ρ_f density of the fluid
τ dimensionless shear stress, $\zeta W^2/(\alpha_f\mu_f)$
Ψ dimensionless streamfunction, ψ/α_f
Ψ_f circulation in the fluid region only
Ψ_w circulation over the entire region
ψ streamfunction
Ω dimensionless vorticity, $\omega W^2/\alpha_f$
ω vorticity
ΔX_i dimensionless mesh size in the porous region next to the interface
δ thickness of a thin region near the interface in which the flow in the porous region is dominated by viscous force.

Subscripts
f fluid region
p porous region.

heat transfer are discussed. A comparison between calculation and experiment is also performed.

2. PROBLEM FORMULATION

2.1. *Governing equations*

We consider a two-dimensional, rectangular enclosure of height H and width W, horizontally divided into the fluid and porous regions as shown in Fig. 1. The fluid is assumed to have constant properties, excluding density in a buoyant term, which is assumed to vary linearly with temperature, i.e. the Boussinesq approximation is utilized. The porous portion of the enclosure is expressed as H'/H and the interface between fluid and porous regions remains horizontal. The upper and lower walls of the enclosure are insulated, while the vertical walls of the enclosure are isothermal; the right-hand side wall is at temperature T_h and the left-hand side at T_c, where $T_h > T_c$.

The Navier–Stokes equation and Darcy's law have been utilized for the fluid motion of the fully-fluid enclosure and for that of the fully-porous enclosure, respectively. If the present analysis uses Darcy's law for the porous region, then velocity and shear stress are discontinuous at the interface. So we use the Brinkman extension of Darcy's law which physically forces a continuity in velocity and shear stress. Such a treatment has already been utilized for flow analysis of a viscous fluid past a permeable body [15, 16].

With the assumptions stated above, the governing equations for this problem are expressed in the following non-dimensional form in terms of streamfunction, vorticity and temperature:

Fluid region

$$U_f\frac{\partial\Omega_f}{\partial X}+V_f\frac{\partial\Omega_f}{\partial Y}=Pr_f\nabla^2\Omega_f-Ra_fPr_f\frac{\partial\theta_f}{\partial Y} \quad (1)$$

$$\nabla^2\Psi_f=-\Omega_f \quad (2)$$

$$U_f \frac{\partial \theta_f}{\partial X} + V_f \frac{\partial \theta_f}{\partial Y} = \nabla^2 \theta_f. \quad (3)$$

Porous region

$$U_p \frac{\partial \Omega_p}{\partial X} + V_p \frac{\partial \Omega_p}{\partial Y} = Pr_f \nabla^2 \Omega_p - (Pr_f/Da)\Omega_p - Ra_f Pr_f \frac{\partial \theta_p}{\partial Y} \quad (4)$$

$$\nabla^2 \Psi_p = -\Omega_p \quad (5)$$

$$U_p \frac{\partial \theta_p}{\partial X} + V_p \frac{\partial \theta_p}{\partial Y} = (\lambda_e/\lambda_f)\nabla^2 \theta_p. \quad (6)$$

The non-dimensional boundary conditions at four walls of the enclosure are

$$\text{at } X = 0: \Psi_p = 0, \quad \Omega_p = -\nabla^2 \Psi_p, \quad \partial \theta_p / \partial X = 0 \quad (7)$$

$$\text{at } X = H/W: \Psi_f = 0, \quad \Omega_f = -\nabla^2 \Psi_f, \quad \partial \theta_f / \partial X = 0 \quad (8)$$

$$\text{at } Y = 0: \Psi_p = \Psi_f = 0, \quad \Omega_p = -\nabla^2 \Psi_p, \quad \Omega_f = -\nabla^2 \Psi_f, \quad \theta_p = \theta_f = 0 \quad (9)$$

$$\text{at } Y = 1: \Psi_p = \Psi_f = 0, \quad \Omega_p = -\nabla^2 \Psi_p, \quad \Omega_f = -\nabla^2 \Psi_f, \quad \theta_p = \theta_f = 1. \quad (10)$$

At the interface ($X = H'/W$), the boundary conditions can not be specified explicitly for streamfunction, vorticity and temperature. Hence, at $X = H'/W$, six continuity conditions will be specified in the following form, coupling the fluid region to the porous region:

$$U_f = U_p \quad (11)$$

$$V_f = V_p \quad (12)$$

$$\tau_f = \tau_p \quad (13)$$

$$P_f = P_p \quad (14)$$

$$\theta_f = \theta_p \quad (15)$$

$$\partial \theta_f / \partial X = (\lambda_e/\lambda_f)\, \partial \theta_p / \partial X. \quad (16)$$

Equations (11)–(14) can be transformed in terms of variables Ψ_f, Ψ_p, Ω_f and Ω_p to obtain an equivalent set of equations, namely

$$\Psi_f = \Psi_p \quad (17)$$

$$\partial \Psi_f / \partial X = \partial \Psi_p / \partial X \quad (18)$$

$$\Omega_f = \Omega_p \quad (19)$$

$$\partial \Omega_f / \partial X = \partial \Omega_p / \partial X - V_p / Da. \quad (20)$$

Derivation of these equations is described in the literature [17]. Equations (1)–(6) together with the boundary conditions [equations (7)–(10) and (15)–(20)] complete the problem definition. These model equations have the advantage of being fully predictive, i.e. there is no need for an experimental fit of any parameter.

The solution of this problem is dependent on the following parameters: H'/H, λ_e/λ_f, H/W, Da, Ra_f and Pr_f. The aspect ratio, the thermal conductivity ratio, the porous portion of the enclosure and Prandtl number were held constant ($H/W = 6$, $\lambda_e/\lambda_f = 1.0$, $H'/H = 0.5$ and $Pr_f = 10$) for all cases considered, since this study is concerned with the development of mathematical model rather than the details of a parametric study. Other parameters were varied in the range $10^3 \leqslant Ra_f \leqslant 10^5$ and $10^{-3} \leqslant Da \leqslant 10^{-5}$.

2.2. *Validity of numerical results*

Numerical solutions of equations (1)–(10) and (15)–(20) were obtained through use of the finite-element method. The solution technique is well described in the literature [17] and has been widely used for natural convection problems [18–20]. The analytical domain was initially discretized using a uniform 60 × 20 mesh of triangular elements.

Figure 2 shows a comparison of the present numerical results and those previously reported; this tests the solution technique. For a fully-fluid enclosure [Fig. 2(a)], at high Rayleigh numbers, the present results are in excellent agreement with the correlation by Churchill [21], which is a generalization of the laminar boundary-layer solution of Bejan [22] including the effect of Prandtl number. In Fig. 2(b), the comparison is for a fully-porous enclosure. The present results agree with those of Bankvall [23].

However, for the case of an enclosure divided into fluid and porous regions, a discretization error may appear through the use of this mesh size. In order to test the effect of mesh size, a smaller mesh size in the vertical direction was employed near the interface, where a sharp shear stress occurs and where the number of

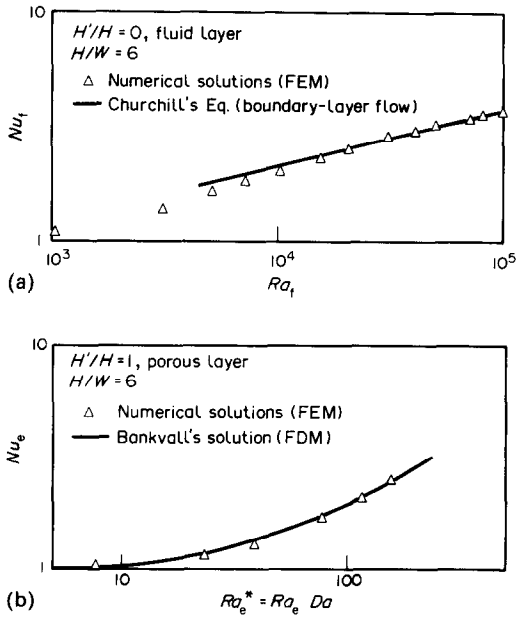

FIG. 2. Comparison of the present calculated Nusselt numbers and those previously reported.

meshes was changed from 60 to 110, but the number of mesh in the horizontal direction was kept constant.

For mesh variation, the temperature field was similar for all mesh sizes, but the flow field was noticeably different. When the dimensionless mesh size next to the interface, ΔX_i is larger than a critical value, the fluid in the fluid region never penetrates into the porous medium, inducing a secondary circulation located at the upper zone in the porous region, which is due to the discretization error, However, when ΔX_i is smaller than the critical value, a part of the fluid in the fluid region penetrates into the porous region and therefore the secondary circulation disappears.

Figure 3 shows the relationship between the size of secondary circulation and the mesh size next to the interface. The critical value of ΔX_i becomes the smaller for the smaller Darcy number. For an example, the critical value for $Da = 10^{-5}$ is about 10^{-3}, which is very small. The reason for this is considered as follows.

The ratio of viscous force to Darcy's resistance in Brinkman's extension of Darcy's law is represented in terms of the width of the enclosure as

$$\frac{\mu_f \nabla^2 v}{(\mu_f v/\kappa)} \sim \frac{\mu_f v/W^2}{\mu_f v/\kappa} \sim \frac{\kappa}{W^2} = Da. \tag{21}$$

When Da is less than 10^{-3}, the viscous force can be neglected except in a region near the interface. However, the flow is dominated by viscous force rather than Darcy's resistance in the porous region next to the interface because of a significant variation of the velocity.

If δ is taken as the thickness of the region near the interface in which the flow in the porous region is dominated by viscous force, changing from W to δ in equation (21) and assuming that the ratio of viscous force to Darcy's resistance is of the order of 1, δ is roughly estimated as

$$\delta/W \sim \sqrt{Da} \tag{22}$$

Thus, when ΔX_i is larger than $\sqrt{Da}$, a remarkable error probably appears in the numerical solution. In fact, the flow patterns significantly change near the values estimated by equation (22) as shown in Fig. 3.

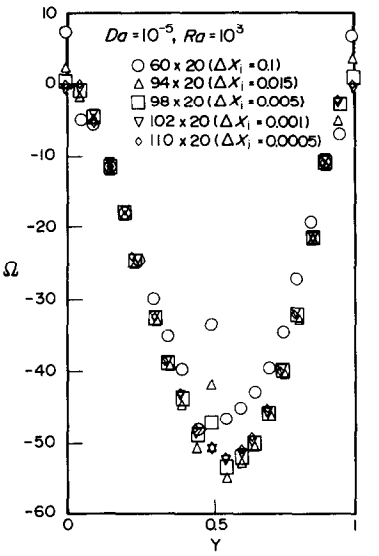

FIG. 4. Effect of mesh size on the vorticity at the interface.

Figure 4 shows the vorticity distributions at the interface for mesh variation. As ΔX_i becomes smaller the vorticity profile and its value scarcely change for mesh variation. The vorticity for a non-uniform 102 $\times$ 20 mesh ($\Delta X_i = 0.001$) is almost equal to that for a non-uniform 110 $\times$ 20 mesh ($\Delta X_i = 0.0005$). Also the value of streamfunction is almost identical for these two mesh sizes, but not shown here. Hence the smaller mesh size with 110 $\times$ 20 as shown in Fig. 5 was used in all the calculation runs.

3. RESULTS AND DISCUSSION OF NUMERICAL CALCULATIONS

3.1. *Flow and temperature fields*

Since the flow pattern is the same for Darcy numbers considered here, the streamlines in the case of $Da = 10^{-3}$ are shown in Fig. 6. For all Rayleigh numbers,

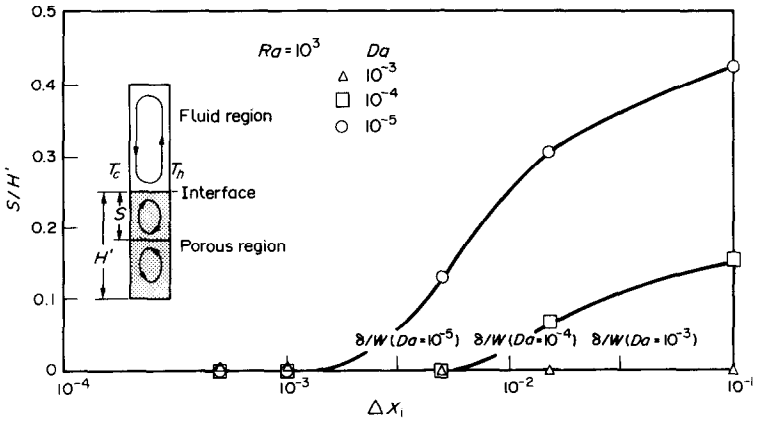

FIG. 3. Effect of mesh size on the flow pattern.

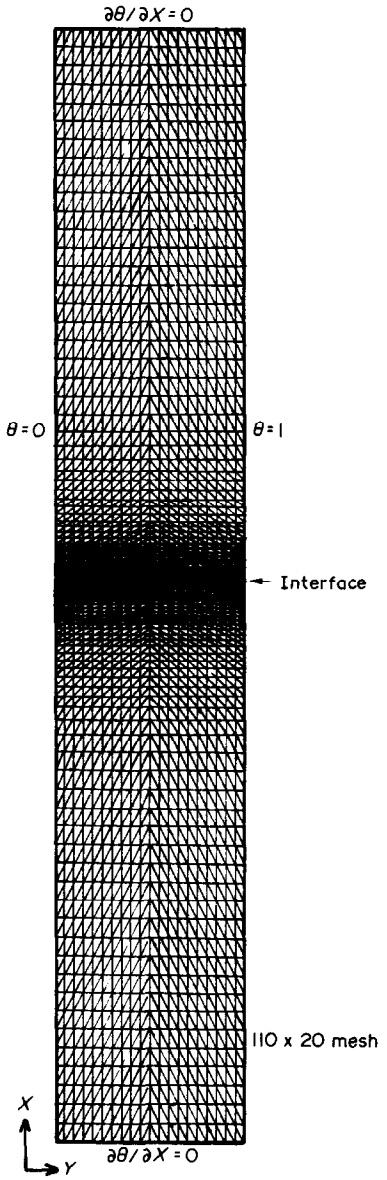

FIG. 5. Finite-element mesh for calculation.

most of the fluid moving downward adjacent to the cold wall in the fluid region goes away from the wall at $x/H = 0.5$ and then moves along the interface towards the hot wall. However, a part of the fluid penetrates into the porous medium. Thus, there are two flow modes for this system: one is a circulation rotating counter-clockwise in the fluid region only and the other is a circulation with the same rotation over the entire region. These flow modes have been also observed in the range $5 \times 10^6 < Ra_f < 3 \times 10^7$ for $Da = 3.5 \times 10^{-6}$ and $\lambda_e/\lambda_f = 1.28$ in previous experiments [13].

The circulation rate in the fluid region only, Ψ_f is almost identical for Darcy numbers considered here, but increases with the Rayleigh number. While the circulation rate over the entire region, Ψ_w decreases with decreasing the Darcy number. Figure 7 shows the ratio of the circulation rate over the entire region to that in the fluid region only. This ratio means a rate of flow penetration from the fluid region into the porous region. The circulation ratio increases with the Rayleigh number, but its relation is not linear. In the range of Rayleigh number considered here, the circulation ratio decreases at a rate which corresponds to a decrease in the Darcy number.

Figure 8 shows the variation of isotherms with the Darcy number at $Ra = 10^5$. The isotherms are almost identical for any Darcy number in the fluid region, but are different in the porous region. This difference is dependent on the variation of the flow penetration rate with the Darcy number.

3.2. *Heat transfer rates for various Darcy numbers*

In the present study, the average Nusselt number is defined as

$$Nu_f = \frac{\text{actual heat transfer rate}}{\text{heat transfer rate by conduction when the entire enclosure is filled with the fluid alone}} \quad (21)$$

and is given in terms of variables of this study as follows

$$Nu_f = (W/H)\left\{(\lambda_e/\lambda_f)\int_0^{H'/W}(\partial\theta_p/\partial Y)\,dX + \int_{H'/W}^{H/W}(\partial\theta_f/\partial Y)\,dX\right\}_{Y=0} \quad (22)$$

where the temperature gradient is evaluated at the cold wall, $Y = 0$.

Figure 9 shows the relation between the Nusselt number and the Rayleigh number. The Nusselt number makes little difference for all Darcy numbers studied and it is smaller than that for the fully-fluid enclosure indicated by the solid line in this figure at high Rayleigh numbers. Normally the Nusselt number increases with the Darcy number and in turn with the permeability. However, the numerical results are contrary to this expectation. So the local Nusselt numbers at the cold wall are shown in Fig. 10 for $Da = 10^{-3}$ and 10^{-5}. The local Nusselt number for $Da = 10^{-3}$ is larger than that for $Da = 10^{-5}$ in the fluid region, while it is smaller in the porous region. The difference in the local Nusselt number for various Darcy numbers is due to a remarkable difference in the flow penetration rate as shown in Fig. 7. However, this difference is almost cancelled when the local Nusselt number is averaged along the cold wall to obtain the averaged Nusselt number.

For such a system consisting of both the fluid and porous regions, the interaction of the natural convection for each region has a strong effect on the flow and temperature fields. In order to estimate quantitatively this interaction, we calculate the apparent Nusselt number $\overline{Nu_f}$ when the natural convection occurs independently in the fluid and porous regions, corresponding to that when an impermeable and adiabatic partition is placed at the

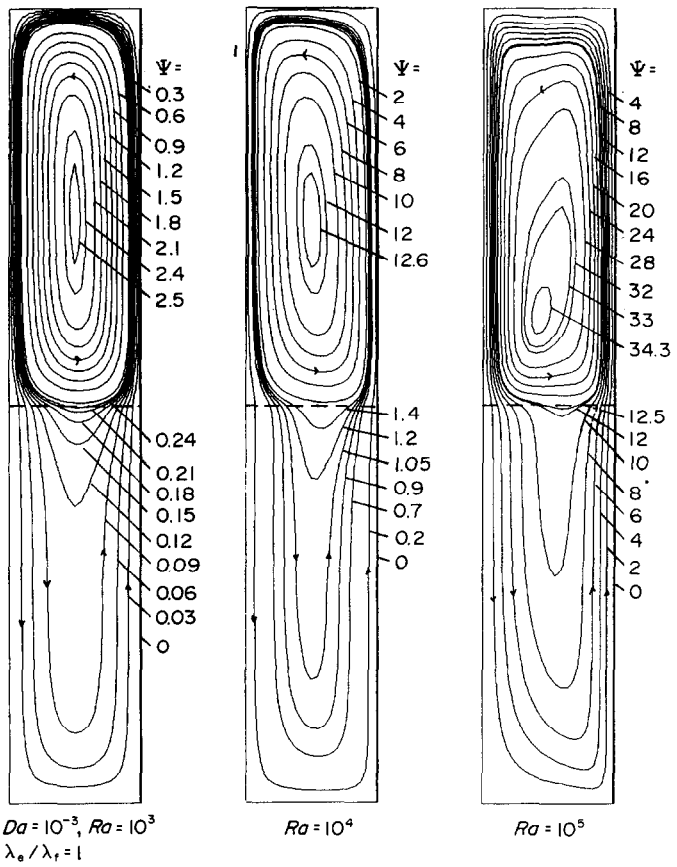

FIG. 6. Variation of streamlines with Rayleigh number for $Da = 10^{-3}$.

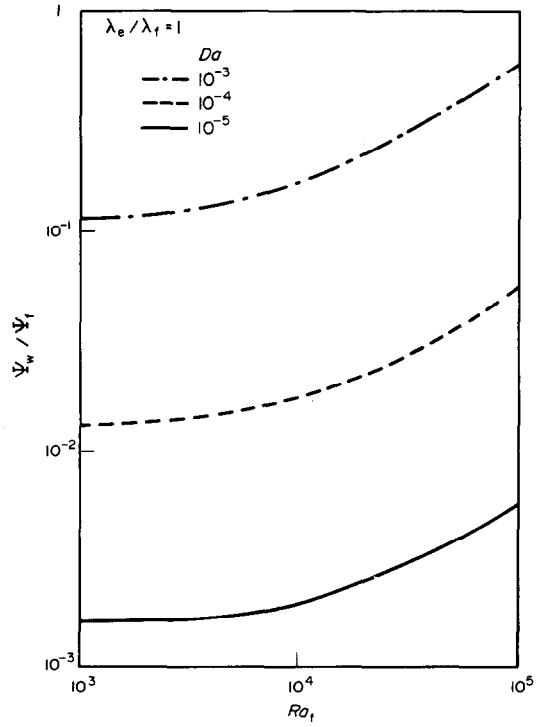

FIG. 7. Variation of flow penetration with Rayleigh number for three different Darcy numbers.

interface. $\overline{Nu}_f$ is calculated by the following equation

$$\overline{Nu}_f = (H'/H)(\lambda_e/\lambda_f)Nu_p^* + (1 - H'/H)Nu_f^*. \quad (23)$$

Figure 11 shows the ratio of Nu_f to $\overline{Nu}_f$. This ratio of Nusselt number decreases with increasing the Rayleigh number. In particular this characteristic becomes significant with an increase in the Darcy number. Thus a decrease in the Nusselt number ratio with increasing Rayleigh number is closely related to the flow penetration rate as shown in Fig. 7.

4. EXPERIMENTS

Since the experimental equipment and procedure have already been described comprehensively [13], they will be reviewed here only briefly. A rectangular enclosure, 5 cm in width and 30 cm in height, whose opposing vertical walls were kept at different temperatures while the upper and lower walls were insulated was used. Silicone oil ($Pr_f \simeq 8000$) was used as the fluid, and the porous medium was composed of glass beads of an average diameter of 3.1 mm. The experiment was carried out for the porous portion of the enclosure $H'/H = 0.5$ in the range $5 \times 10^4 < Ra_f < 3 \times 10^5$. We observed the flow pattern by the tracer consisting of iodine solution or small particles, and also

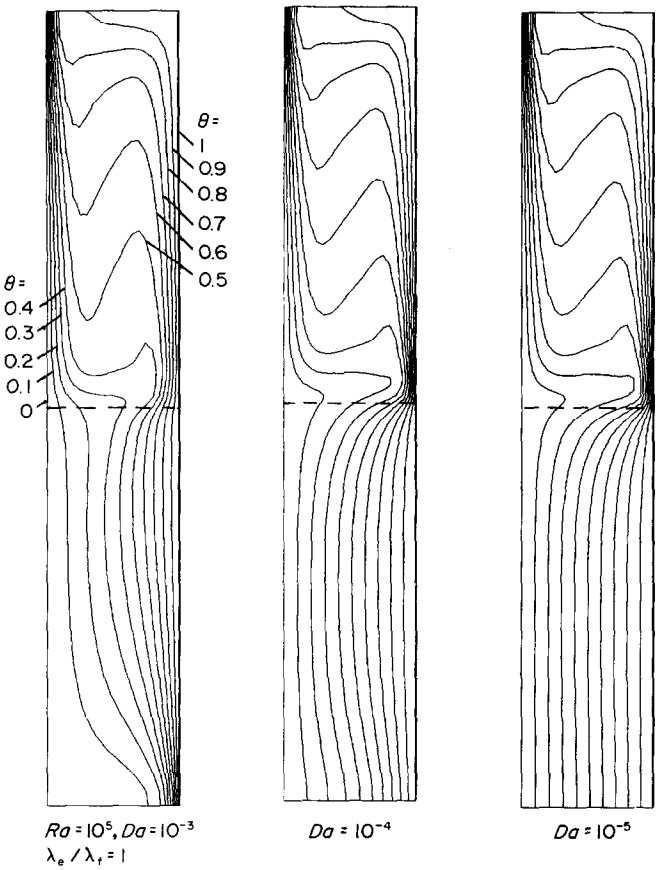

FIG. 8. Variation of isotherms with Darcy number for $Ra = 10^5$.

measured the temperature distribution and the heat transfer rate through the enclosure.

Figure 12(a) shows a photograph of the flow visualization in the fluid region. A circulation over the fluid region and twin secondary circulations are clearly recognizable. On the other hand, in the porous region, the tracer consisting of iodine solution injected through a port of the lower wall of the enclosure spread over the porous region at a low speed and thus the flow in the porous region is not clearly recognizable. Figure 12(b) shows the corresponding numerical streamlines by the analytical model described above. The agreement between the experiment and the analysis is good in the fluid region but is not clear in the porous region. The reason for this is that the flow rate in the porous region is much smaller than that in the fluid region, as seen from the ratio of Ψ_w to Ψ_f indicated in Fig. 12(b).

Figure 13 shows a comparison of experimental and

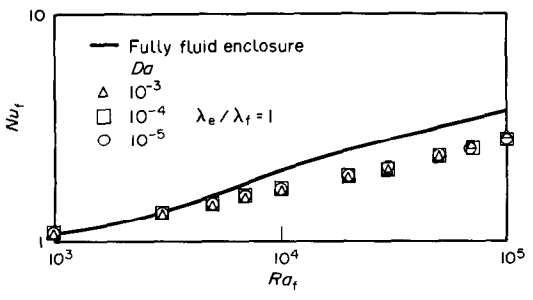

FIG. 9. Variation of Nusselt numbers with Rayleigh number for three different Darcy numbers.

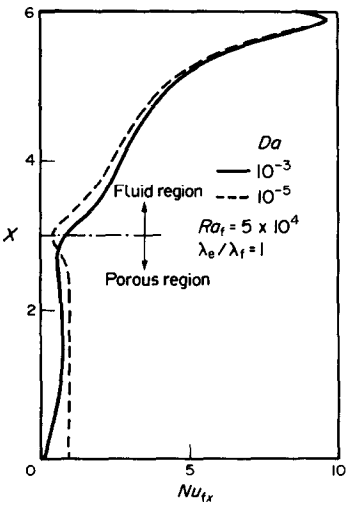

FIG. 10. Local Nusselt number distributions for two different Darcy numbers.

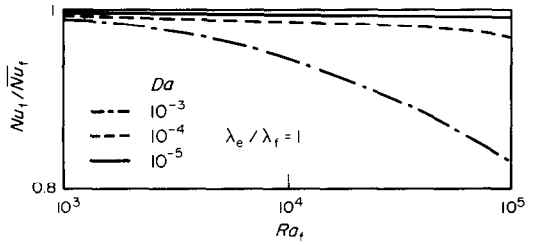

FIG. 11. Variation of Nusselt number ratios with Rayleigh number for three different Darcy numbers.

numerical temperature distributions at each horizontal section in the enclosure. The numerical distributions are found to be in very good agreement with the experimental data for both the fluid and porous regions. The temperature distribution near the lower wall ($x/H = 0.02$) is identical with that of the heat conduction. This result indicates that the flow rate in the porous region is extremely small.

Figure 14 shows a comparison of experimental and

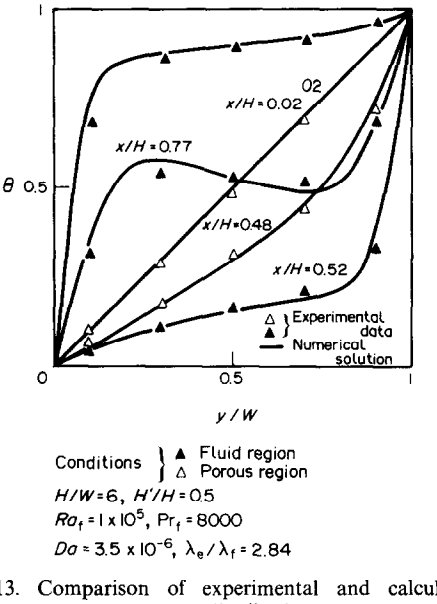

FIG. 13. Comparison of experimental and calculated temperature distributions.

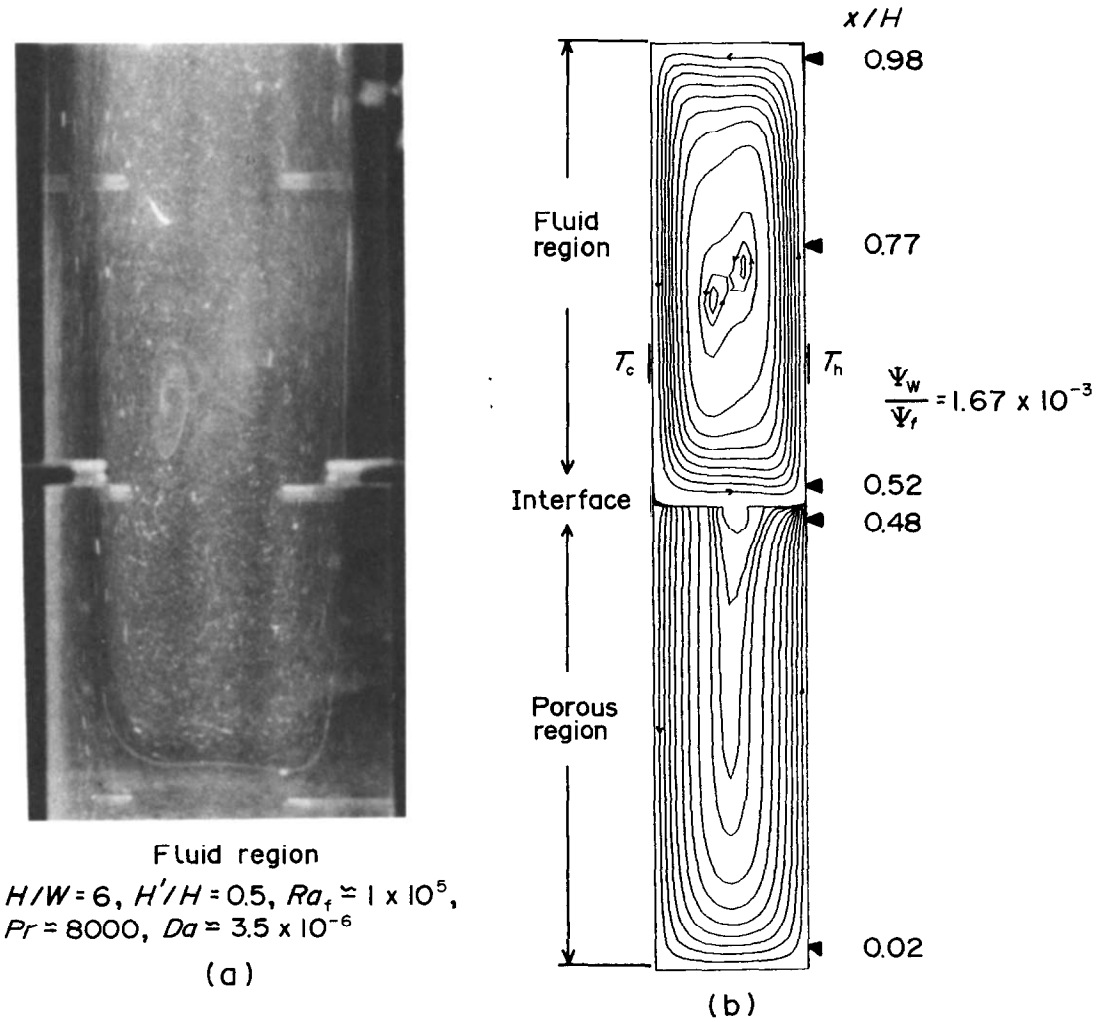

FIG. 12. Comparison of experimental and calculated flow patterns.

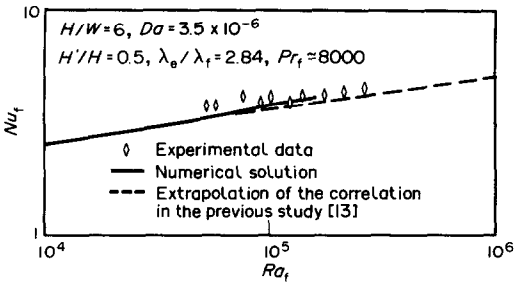

FIG. 14. Comparison of experimental and calculated Nusselt numbers.

numerical Nusselt numbers. The agreement between the experiment and the numerical solution is good; the experimental data are also in agreement with the correlation indicated by the dotted line—an extrapolation of the correlating equation for higher Rayleigh numbers ($7.3 \times 10^5 < Ra_f < 2.6 \times 10^7$) presented by the previous experimental study [13].

5. CONCLUSIONS

Natural convection heat transfer in a rectangular enclosure horizontally divided into fluid and porous regions was analyzed numerically. The Navier–Stokes equation and Brinkman's equation were used for the fluid motion in the fluid region and for that in the porous region, respectively. These equations were solved by the finite-element method. The flow and temperature fields varied with the Rayleigh number and the Darcy number. In particular, the rate of flow penetration from the fluid region into the porous region considerably varied with the Darcy number. The numerical results agreed well with the experiments.

In this study, the validity of the analytical model has not yet been completely performed, because the comparison between the analytical model and the experiment is made under a condition in which the heat transfer in the porous region is mainly dominated by heat conduction. In the future it is hoped that the numerical calculation will be expanded to higher Rayleigh numbers than those studied in this work.

Acknowledgements—This study was supported by special projects (Cryogenic-Chemical Engineering) of Hiroshima University. The authors would like to thank a referee from this journal for useful suggestions in improving the original version of this paper.

REFERENCES

1. S. Ostrach, Natural convection in enclosures, *Adv. Heat Transfer* **8,** 161–227 (1972).
2. I. Catton, Natural convection in enclosures, *Proc. 6th Int. Heat Transfer Conference*, Vol. 6, pp. 13–43 (1978).
3. H. Ozoe, K. Yamamoto, S. W. Churchill and H. Sayama, Three-dimensional numerical analysis of laminar natural convection in a confined fluid heated from below, *J. Heat Transfer* **98,** 202–207 (1976).
4. P. Cheng, Heat transfer in geothermal system. *Adv. Heat Transfer* **14,** 1–105 (1979).
5. A. Bejan, A synthesis of analytical results for natural convection heat transfer across rectangular enclosures, *Int. J. Heat Mass Transfer* **23,** 723–726 (1980).
6. W. Knight and M. E. Palmer, Simulation of free convection in multiple fluid layers in an enclosure by finite differences. In *Numerical Properties and Methodologies in Heat Transfer*, pp. 305–319. Hemisphere, Washington, DC (1983).
7. T. Kimura, N. Heya, M. Takeuchi and H. Isobe, Natural convection of fluids with stratified two layers in a rectangular enclosure (numerical analysis taking the boundary tension into consideration), *Proc. 20th National Heat Transfer Symposium of Japan*, pp. 118–120 (1983).
8. T. Kimura, N. Heya, M. Takeuchi and H. Isobe, Natural convection heat transfer in rectangular enclosure contained fluids with stratified two layers, *Proc. 21st National Heat Transfer Symposium of Japan*, pp. 136–138 (1984).
9. R. Mackibbin and P. A. Tyvand, Anisotropic modeling of thermal convection in multilayered porous media, *J. Fluid Mech.* **118,** 315–339 (1982).
10. D. Poulikakos and A. Bejan, Natural convection in vertically and horizontally layered porous media heated from the side, *Int. J. Heat Mass Transfer* **26,** 1805–1814 (1983).
11. C. W. Somerton and I. Catton, On the thermal instability of superposed porous and fluid layers, *J. Heat Transfer* **104,** 160–165 (1982).
12. T. W. Tong and E. Subramanian, Natural convection in rectangular enclosures partially filled with a porous medium, *Proc. ASME–JSME Joint Conference in Thermal Engineering*, pp. 331–338 (1983).
13. T. Nishimura, T. Takumi, Y. Kawamura and H. Ozoe, Experiments of natural convection heat transfer in rectangular enclosures partially filled with particles, *Kagaku Kogaku Ronbunshu* **11,** 405–410 (1985).
14. H. C. Brinkman, A calculation of the viscous force exerted by a flowing fluid on a dense swarm of particles, *Appl. Sci. Res.* **A1,** 27–34 (1949).
15. K. Nandakumar and J. H. Masliyah, Laminar flow past a permeable sphere, *Can. J. chem. Engng.* **60,** 202–211 (1982).
16. K. Yamamoto, Flow of viscous fluid at small Reynolds numbers past a porous body, *J. phys. Soc. Japan* **34,** 814–819 (1973).
17. T. Takumi, Experiment and theory of natural convection heat transfer in rectangular enclosures partially filled with particles. M. thesis, Hiroshima University (1984).
18. B. Tabarrok and R. C. Lin, Finite element analysis of free convection flows, *Int. J. Heat Mass Transfer* **20,** 945–952 (1977).
19. C. E. Hickox and D. K. Gartling, A numerical study of natural convection in a horizontal porous layer subjected to an end to end temperature difference, *J. Heat Transfer* **103,** 797–802 (1981).
20. T. Nishimura, T. Takumi, Y. Kawamura and H. Ozoe, Analysis of natural convection heat transfer at the wall of packed beds with voidage variation, *Kagaku Kogaku Ronbunshu* **10,** 648–652 (1984).
21. S. W. Churchill, Free convection in layers and enclosures. In *Heat Exchanger Design Handbook*, Chap. 2.5.8. Hemisphere, Washington, DC (1983).
22. A. Bejan, Note on Gill's solution for free convection in a vertical enclosure, *J. Fluid Mech.* **90,** 561–568 (1979).
23. C. G. Bankvall, Natural convection in vertical permeable space, *Wärme-u. Stoffübertr.* **7,** 22–30 (1974).

ANALYSE NUMERIQUE DE LA CONVECTION NATURELLE DANS UNE ENCEINTE RECTANGULAIRE DIVISEE HORIZONTALEMENT EN DES REGIONS POREUSE ET FLUIDE

Résumé—On décrit une étude analytique de la convection naturelle dans une enceinte rectangulaire divisée horizontalement en deux régions poreuse et fluide. L'équation de Navier-Stokes gouverne le mouvement du fluide dans la région du fluide, tandis que l'extension de la loi de Darcy est supposée être valable dans la région poreuse. Ces équations sont résolues par une méthode aux éléments finis dans le domaine $10^3 \leqslant Ra \leqslant 10^5$ et $10^{-3} \leqslant Da \leqslant 10^{-5}$. L'expérience est conduite pour une enceinte rectangulaire couplée avec du silicone et des billes de verre. On montre que la configuration de l'écoulement, la distribution de température et le nombre de Nusselt obtenus par le calcul numérique prédisent correctement les données expérimentales.

NUMERISCHE UNTERSUCHUNG DER NATÜRLICHEN KONVEKTION IN EINEM RECHTECKIGEN HOHLRAUM MIT WAAGERECHTER TRENNUNG ZWISCHEN SCHÜTTUNG UND FLUID

Zusammenfassung—Der Artikel beschreibt eine analytische Untersuchung des Wärmeübergangs bei laminarer natürlichen Konvektion in einem rechteckigen Hohlraum mit horizontaler Trennung von Schüttung und Fluid. Die Navier–Stokes-Gleichungen beschreiben die Bewegung des Fluids im Gebiet des reinen Fluids, während Brinkman's Erweiterung des Darcy-Gesetzes als gültig für die Schüttung angenommen wird. Die Gleichungen werden mit einem Finite-Elemente-Verfahren gelöst im Bereich von $10^3 \leqslant Ra_f \leqslant 10^5$ und $10^{-3} \leqslant Da \leqslant 10^{-5}$. Eine experimentelle Untersuchung wird ebenfalls durchgeführt an einem rechteckigen Behälter, der mit Silikonöl und Glaskugeln gefüllt ist. Es wird gezeigt, daß das Strömungsbild, die Temperaturverteilung und die Nusselt-Zahl, die man aus den numerischen Berechnungen erhält, die experimentellen Werte zufriedenstellend vorhersagen.

ЧИСЛЕННЫЙ АНАЛИЗ ЕСТЕСТВЕННОЙ КОНВЕКЦИИ В ПРЯМОУГОЛЬНОМ ОБЪЕМЕ С ГОРИЗОНТАЛЬНЫМ ДЕЛЕНИЕМ НА ЖИДКУЮ И ПОРИСТУЮ ОБЛАСТИ

Аннотация—Аналитически изучается ламинарный естественноконвективный теплоперенос в прямоугольной полости с горизонтальным делением на жидкую и пористую области. Движение в области жидкости определяется уравнением Навье–Стокса. В пористой области применяется обобщение Бринкмана для закона Дарси. Уравнения решаются методом конечных элементов при $10^3 \leqslant Ra_f \leqslant 10^5$ и $10^{-3} \leqslant Da \leqslant 10^{-5}$. Эксперименты проводятся с прямоугольной емкостью, заполненной силиконовым маслом и стеклянными шариками. Показано, что рассчитанные режим течения, распределение температуры и число Нуссельта удовлетворительно соответствуют экспериментальным данным.